Eighth Australasian Fluid Mechanics
Conference, University of Newcastle,
N.S.W., 28 November/2 December 1983.

SOME NEW APPLICATIONS OF LINEARIZED AIRFOIL THEORY

G.V. PARKINSON AND G.D. WATT

DEPARTMENT OF MECHANICAL ENGINEERING

UNIVERSITY OF BRITISH COLUMBIA, VANCOUVER, B.C. V6T 1W5 CANADA

SUMMARY New linearized theory is presented for pitching moment characteristics of two-element airfoils and for a correction method for a new type of slotted-wall wind tunnel. Comparisons with exact numerical calculations and with experimental data show good agreement with predictions of the linearized theory.

1 INTRODUCTION

Despite the universal adoption of numerical surface-singularity methods, often mated with boundary-layer calculations, for the prediction of the aerodynamic properties of low speed airfoils there is still an important role to be played by analytic linearized theory. Because of its relatively simple equations, which lend themselves to rapid computation on a programmable hand or desk calculator, and its capability of superposition of effects, it can be a valuable tool for the aerodynamicist. In this paper, two applications of thin airfoil theory currently under development in the aerodynamics laboratory at the University of British Columbia are described. The first is an extension of the theory to two-element airfoils, either an airfoil with slotted flap or with leading-edge slat. The second application is to a residual correction theory for a new form of low-correction wind tunnel test section for two-dimensional airfoil testing.

2 TWO-ELEMENT AIRFOIL PITCHING MOMENT COMPARISONS

Thin airfoil theory has been successfully extended, by the authors in Watt and Parkinson, 1983 [WP,1983], to uncambered tandem wings as shown in Figure 1a. Here, the relative slot length, f-s, is variable between 0 and 1; the front element, or airfoil, is of relative length s; the rear element, or flap, of relative length 1-f. The potential flow about this configuration, for arbitrary but small values of α and η, is solved for by making the classical thin airfoil theory boundary condition linearization [Glauert, 1926]. The solution ignores thickness effects since thin airfoil theory predicts no effect on lifts or pitching moments by thickness for in-line airfoil elements. The solution is analytical and involves the readily calculable theta functions (elliptic functions). Expressions for lift and pitching moment coefficients are obtained using the Blasius equations. Although some of these expressions reduce to simple algebraic functions of the initial geometry, s and f, in general, they are functions of complete and incomplete elliptic integrals and functions. Nevertheless, using the efficient theory of the theta functions, overall lift and airfoil and flap lift coefficients, overall moment and airfoil and flap moment coefficients can be calculated on a TI Programmable 59 hand calculator in about half a minute. These coefficients are calculated in terms of their linear variation with α and η, a characteristic result, in thin airfoil theory, of the boundary condition linearization. The coefficients can be shown to reduce to the classical one-element thin airfoil theory coefficients in the limits as f-s goes to 0 or 1.

WP [1983] presents lift coefficients and overall moment coefficients and makes lift comparisons between thin airfoil theory and numerical potential flow theory. In this paper, the remaining airfoil and flap moment coefficients are presented and the same comparisons are then made for moment. The convention used is that overall lift and moment are nondimensionalized by s + 1 - f

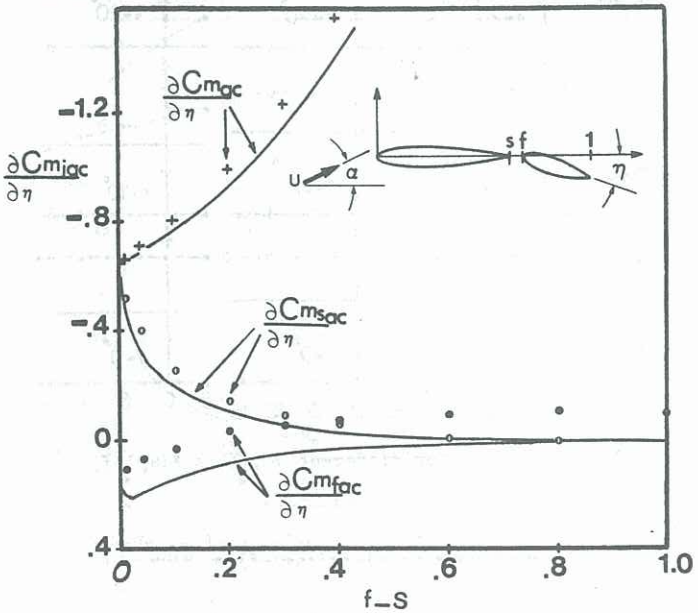

(a) $\partial C_{m_{i_{ac}}}/\partial\eta$ vs. f-s

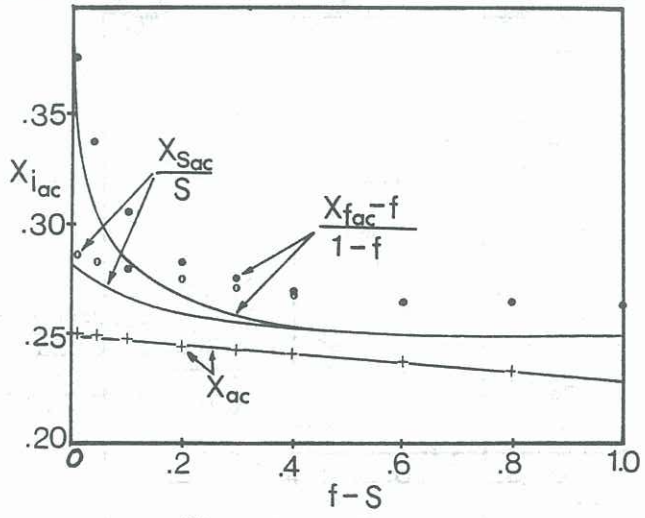

(b) $X_{i_{ac}}$ vs. f-s

Figure 1 Variation of aerodynamic center functions with f-s; (1-f)/(s+1-f) = .2308

+,o,● numerical theory, NACA0015 sections
——— linearized theory

and $(s+1-f)^2$ to form their respective coefficients C_ℓ and C_{m_o}; airfoil lift and moment by s and s^2 to form C_{ℓ_s} and $C_{m_{s_o}}$; flap lift and moment by 1-f and $(1-f)^2$ to form C_{ℓ_f} and $C_{m_{f_o}}$. Moment coefficients correspond to moments about the airfoil leading edge for C_{m_o} and $C_{m_{s_o}}$, and to moment about the flap leading edge for $C_{m_{f_o}}$. The airfoil moment coefficient variation with α and η is:

$$\frac{\partial C_{m_{s_o}}}{\partial \alpha} = \frac{-\pi}{2s^2}\left\{[1-(f-s)(3f+s-2)](1-\Sigma_f)+(3f+s-5)G_1 + (3f-s-1)\,G_2\right\} \qquad (1a)$$

$$\frac{\partial C_{m_{s_o}}}{\partial \eta} = \Sigma_f \frac{\partial C_{m_{s_o}}}{\partial \alpha} - \frac{\pi}{2s^2}\left\{[(s+1+f)G_2 - (3f+s-1)G_1](1-\Sigma_f) - \frac{4(1-f)}{f-s}\,G_1^2 - (G_2-G_1)^2\right\} \qquad (1b)$$

and $C_{m_{f_o}}$ is then easily obtained from C_{m_o}, $C_{m_{s_o}}$, and C_{ℓ_f}. Σ_f, G_1, and G_2 are elliptic functions of s and f and are given in WP [1983].

For comparison purposes, it is convenient to use aerodynamic centers and their associated pitching moments, where:

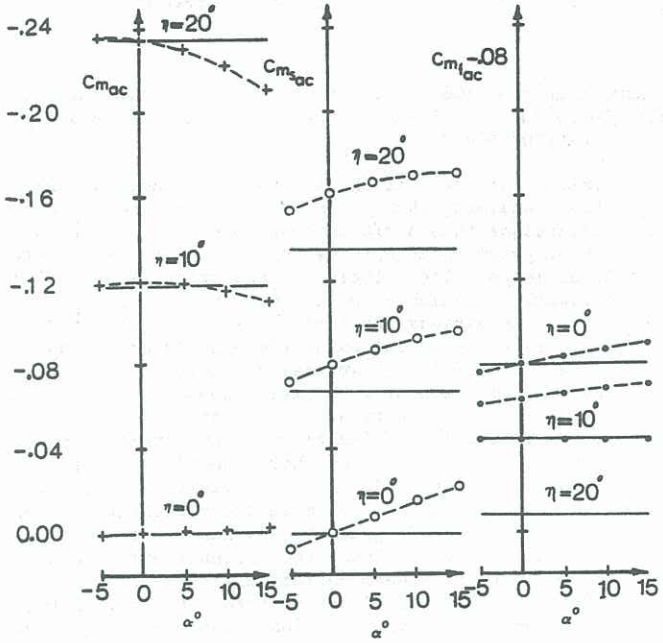

(a) $C_{m_{i_{ac}}}$ vs. α for different η; (f-s)/(s+1-f) = .025

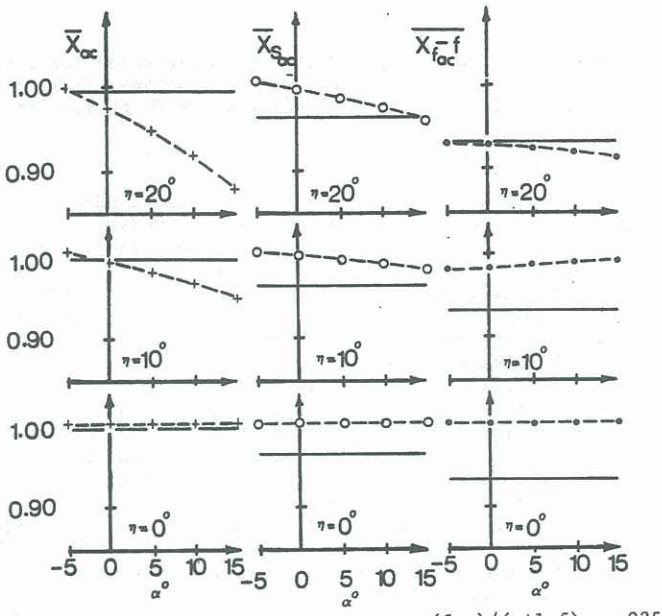

(b) $X_{i_{ac}}$ vs. α for different η; (f-s)/(s+1-f) = .025

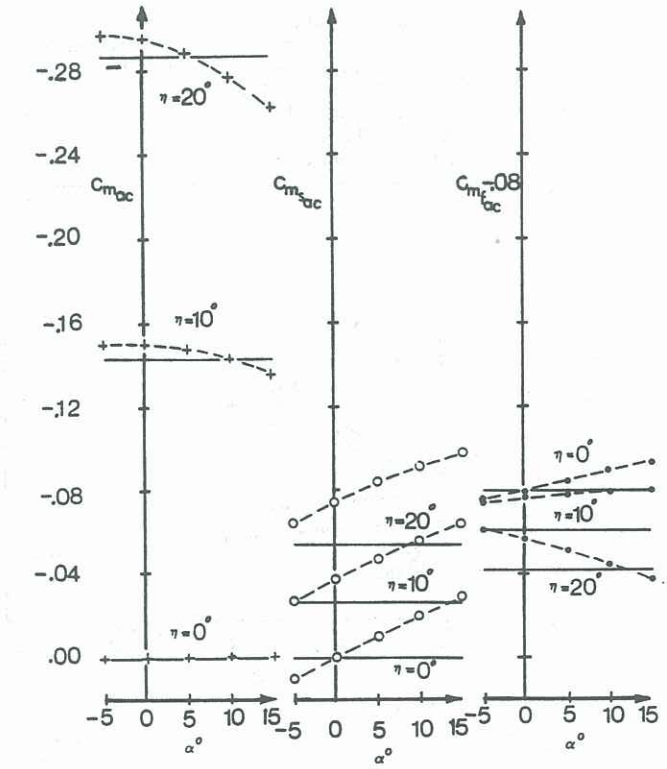

(c) $C_{m_{i_{ac}}}$ vs. α for different η; (f-s)/(s+1-f) = .154

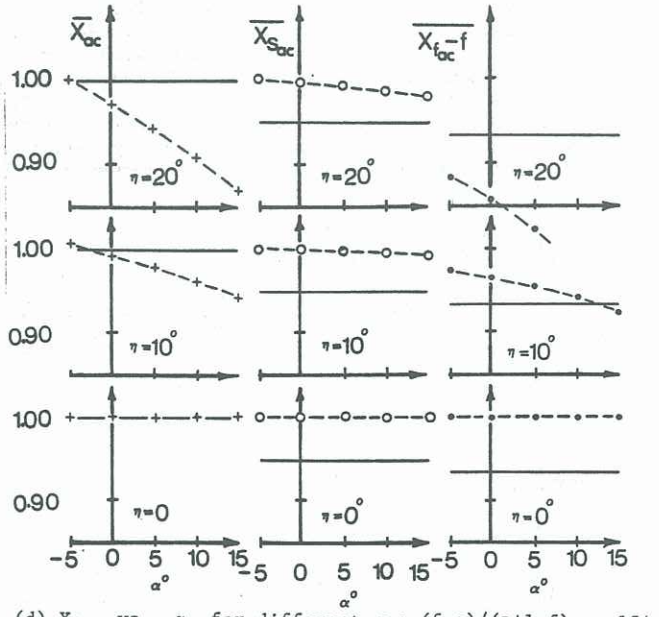

(d) $X_{i_{ac}}$ vs. α for different η; (f-s)/(s+1-f) = .154

Figure 2 Variation of aerodynamic center functions with α and η; (1-f)/(s+1-f) = .2308

+--o--● numerical theory, NACA0015 sections

——— linearized theory

$$C_{m_{i_{ac}}} = C_{m_{i_o}} + (C_{\ell_i} \cos\alpha + C_{d_i} \sin\alpha) X_{i_{ac}}/c_i \qquad (2)$$

where c_i is the pertinent chord length and where:

$$\partial C_{m_{i_{ac}}} / \partial\alpha = 0 \qquad (3)$$

defines $X_{ac}/(s+1-f)$, $X_{s_{ac}}/s$, and $(X_{f_{ac}}-f)/(1-f)$.

Thin airfoil theory predictions for the aerodynamic centers and for the variations of the three aerodynamic center pitching moment coefficients with η, can be obtained by applying Equation (3) to Equation (2) and then using Equations (1) and the other aerodynamic coefficient variations with α and η presented in WP [1983]. Note that, for Equation (2), thin airfoil theory takes $\cos\alpha = 1$ and predicts zero drag for individual airfoil elements as well, of course, as for the overall drag. Of particular interest is the result:

$$X_{ac} = \frac{-\partial C_{m_o}}{\partial\alpha} \frac{s+1-f}{\partial C_\ell/\partial\alpha} = \frac{1}{4} - (f-s)\left(\frac{1}{4} - \frac{1-f}{s+1-f}\right) \qquad (4)$$

The numerical potential flow calculations use a vortex surface-singularity method [Kennedy, 1977] employing the stream function as fundamental variable. For the present calculations its accuracy has been improved upon. All aerodynamic coefficients are now calculated by applying the Blasius equations for lift and moment to the complex velocity, obtained by taking the derivative of the complex potential which is formulated from the stream function representation and its harmonic conjugate. The method provides particularly dramatic increases in accuracy when calculating airfoil element drag, probably because it guarantees an overall drag of zero.

Numerical calculations of the aerodynamic center functions use Equations (2) and (3). Variations of coefficients with α and η are approximated by assuming a straight line variation over a 1° interval, centered on the α or η of interest. For a proper comparison of $C_{m_{i_{ac}}}$, the thin airfoil theory value for $X_{i_{ac}}$ is used in Equation (2). NACA 0015 airfoil elements are used and are represented by 80 straight line segments per element.

Figures 1 and 2 compare thin airfoil theory predictions with the numerical theory. Figure 1 shows variation of the aerodynamic center functions with f-s for a constant flap chord to total chord ratio of 23%. Numerical calculations are for $\alpha = \eta = 0°$. Thin airfoil theory predictions are quite good for the overall aerodynamic center functions and are acceptable for the individual airfoil element functions. Of course, the latter have been expanded somewhat by the choice of the nondimensionalizing length.

Figures 2a and 2b also show variations of the aerodynamic center functions but with varying α and η values and for a constant slot of 2.5%. Figures 2c and 2d do the same for a slot size of 15.4%, an effective midpoint in slot sizes. In the Figures $\bar{X}_{i_{ac}}$ is $X_{i_{ac}}$ divided by its numerical value at $\alpha = \eta = 0°$. Again, agreement is very good for the overall functions, although less so at high values of $\alpha+\eta$ (Here the Equation (2) definition of $X_{i_{ac}}$ loses some meaning, however, since for large η's there is appreciable vertical as well as horizontal movement of the aerodynamic centers.). Individual airfoil element moments exhibit less agreement but in proportion to their decreasing magnitudes and, therefore, importance. Except for $X_{f_{ac}}$ at large η's, individual airfoil element aerodynamic center thin airfoil theory predictions are within 7% of the numerically calculated values.

3 WIND TUNNEL BOUNDARY CORRECTIONS IN LOW SPEED AIRFOIL TESTING

3.1 Conventional Practice

In low speed wind tunnel testing the proximity of the flow boundaries to the test model causes a disturbance velocity field which alters the model loadings, increasing them in tunnels with solid walls and reducing them in open jets. For these conventional tunnels simple formulas, derived from small-disturbance potential flow theory, are commonly used to calculate corrections to test data for effects of the flow boundaries [Pope and Harper, 1966]. These corrections are satisfactorily accurate when the test models are relatively small. However, in two-dimensional airfoil testing Reynolds number simulation typically requires airfoils to be as large as possible, so that the data corrections may become unacceptably large in the relatively small wind tunnels common to university laboratories.

One approach to this problem is to design tunnel test sections with partly solid, partly open boundaries in order to take advantage of the above-mentioned opposite effects of the two boundary types on loadings. A design of this class has been produced [Williams, 1975] and is under development in the authors' laboratory.

3.2 The Tolerant Tunnel

Known as the Tolerant Tunnel, this test section configuration has a solid wall opposite the pressure side of the test airfoil and a row of airfoil-shaped transverse slats replacing the wall opposite the suction side, as shown in the inset to Figure 3. On this side of the test airfoil the constrained streamline pattern is relieved as streamlines pass between the slats into the plenum upstream and back into the test section downstream. The final flow boundary inside the plenum is the free shear layer from the upstream test section corner. The use of a solid wall opposite the pressure side of the test airfoil avoids the problem of a corresponding free shear layer inside the test section.

Numerical surface-singularity potential flow modelling was used to determine a suitable value of open-area ratio $r = g/(c+g)$ useable over as large a range as possible of relative test model size C_o/H (See Figure 3 for the definition of terms), and it was found that wall slat configurations with $.6 \leq r \leq .8$ should give low-correction data over a considerable range of test airfoil profiles, sizes, and angles of attack α. This was confirmed experimentally, so that the Tolerant Tunnel would be a suitable design for a small ($H \leq 1m$) wind tunnel. In airfoil tests with small C_o/H no corrections to the data would be needed. For larger C_o/H simple formulas, derived by the same methods used for the corrections in conventional tunnels, could be used to calculate the small residual corrections, as follows.

3.3 Theory for Residual Corrections

The conventional theory assumes two dimensional incompressible irrotational flow and represents a lifting airfoil by a single vortex at the quarter-chord point, or by an equivalent distribution of vortices over the chord. Effects of airfoil thickness are represented by a distribution of doublets over the chord. Linearization requires retaining only the linear terms in α and in the disturbance velocities u' and v' in the x- and y-directions, and up to quadratic terms in (C_o/H). Test section boundary conditions are applied at $y = \pm H/2$, where the origin is taken at the test airfoil quarter-chord point. On a solid boundary $v' = 0$ and along a jet boundary or free streamline it is assumed $u' = 0$, corresponding to constant undisturbed pressure.

In the present version of the theory the test section is assumed infinitely long and the upper boundary, after linearization, is assumed to be a free streamline with imbedded point vortices representing the wall slats. Since the boundary condition $v' = 0$ is not met on the solid elements of the upper boundary, this model gives correction formulas that become valid as the slats become vanishingly small ($r \to 1$), but are increasingly in error as $r \to 0$, the solid wall limit. The lift correction formula is given here as the ratio

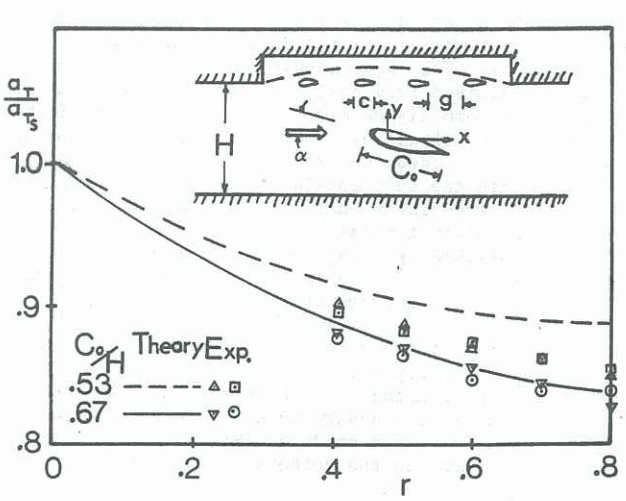

Figure 3 Effect of Wall Open Area Ratio on Lift

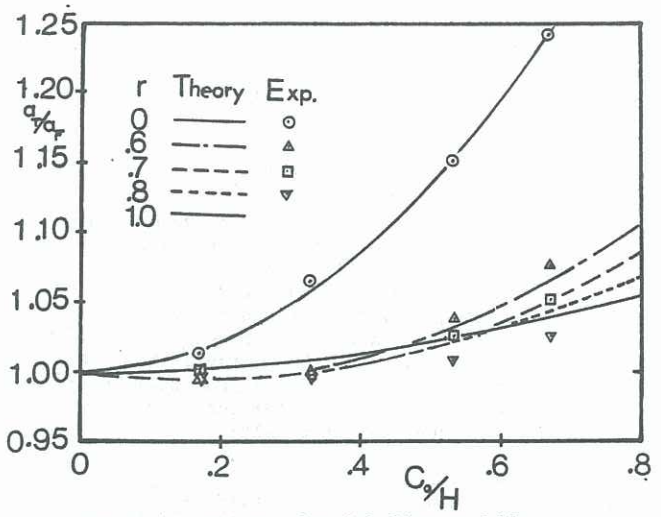

Figure 4 Effect of Model Size on Lift

of uncorrected $(\ )_T$ to corrected or free-air $(\ )_F$ lift-curve slope $a = dC_L/d\alpha$:

$$\frac{a_T}{a_F} = 1 - M(1-r)\left(\frac{C_o}{H}\right) + \frac{\pi^2}{96}\left(1-\frac{\lambda}{2}\right)\left(\frac{C_o}{H}\right)^2. \qquad (5)$$

In Equation (5) the first term represents the effect of the disturbance velocity field created by the wall slats as they develop lift due to the local angles of attack arising from the original disturbance velocity field of the lifting test airfoil. The factor $M = \frac{\pi}{4}\left(\frac{\pi}{4} - \frac{1}{2}\ln 2\right)$ also represents the effect of the images of the boundary vortices needed to simultaneously satisfy $v' = 0$ on the solid wall and $u' = 0$ on the free streamline. The second term gives the effect of the corresponding images of the vortex and doublets representing the test airfoil, and λ is the shape factor for the airfoil.

If the linearized upper boundary condition had been solved exactly, the equation for lift curve slope would have the form:

$$\frac{a_T}{a_F} = 1 - F(1-r)\left(\frac{C_o}{H}\right) + G(1-r)\left(\frac{C_o}{H}\right)^2 \qquad (6)$$

where $F(0) = F(1) = 0$; $G(0) = \frac{\pi^2}{96}\left(1-\frac{\lambda}{2}\right)$; and $G(1) = \frac{\pi^2}{24}(1+\lambda)$ to satisfy the known limits for two solid walls ($r = 0$) and a solid wall opposite a free streamline ($r = 1$). Since $(1-r)$ is small for configurations of interest, $G(1-r)$ can be replaced by the constant and linear terms of its series expansion, while $F(1-r)$ requires the linear and quadratic terms. The final form is:

$$\frac{a_T}{a_F} = 1 - M\left\{(1-r)-(1-r)^2\right\}\left(\frac{C_o}{H}\right) + \frac{\pi^2}{192}\left\{(2-\lambda) + (6+9\lambda)(1-r)\right\}\left(\frac{C_o}{H}\right)^2. \qquad (7)$$

3.4 Comparisons with Experiment

In Figures 3 and 4 two comparisons are made of the predictions of the correction theory (Equation 7) with experimental data obtained by Williams. In Figure 3 the ratio a_T/a_{T_s}, where a_{T_s} is the uncorrected lift curve slope in the presence of solid walls, is plotted against r for two fixed values of C_o/H. This presentation tends to eliminate the effect on the experimental data of the interaction between the boundary layers on the test airfoil and the end walls, which increases with C_o/H. The data were obtained for two different airfoil profiles and two sizes of wall slat. The theory is seen to give the correct trends and is in quite good quantitative agreement with the data.

In Figure 4 a_T/a_F is plotted against C_o/H for several fixed values of r. The experimental data are for a NACA0015 airfoil at a Reynolds number of 10^6, and the data points for the two higher values of C_o/H have been adjusted to compensate for the above-mentioned effect of end wall boundary layers by raising the solid-wall data to agree with the solid-wall theoretical curve (an agreement well established in other laboratories), and raising the other data points for the same C_o/H in proportion. Again the theoretical curves are seen to be in quite good agreement with the data for the slatted-wall configurations, particularly for r = 0.7.

4 DISCUSSION

These new applications of linearized airfoil theory are shown, by the above comparisons with exact numerical potential flow theory or with experimental data, to produce sufficiently accurate predictions to make them useful in engineering practice while providing simple formulas for calculation or for visualization of relative effects. Work is continuing to extend the two-element theory for effects of camber, thickness, and overlap, and to refine the boundary condition for the slatted boundary in the tunnel correction theory.
Finally, the authors wish to acknowledge support of the research by a grant from the Natural Sciences and Engineering Research Council of Canada.

5 REFERENCES

GLAUERT, H. [1926] The Elements of Aerofoil and Airscrew Theory. Cambridge.

KENNEDY, J.L. [1977] The Design and Analysis of Airfoil Sections. Ph.D. Thesis, University of Alberta.

POPE, A. and HARPER, J.J. [1966] Low Speed Wind Tunnel Testing. Wiley, New York.

WATT, G.D. and Parkinson, G.V. [1983] On the Application of Linearized Theory to Multi-Element Aerofoils. Part I: Tandem Flat Plate Aerofoils. Aero. Quart., 34, pp. 46-60.

WILLIAMS, C.D. [1975] A New Slotted-Wall Method for Producing Low Boundary Corrections in Two-Dimensional Airfoil Testing. Ph.D. Thesis, University of British Columbia.